ACS Catalysis

pubs.acs.org/acscatalysis Research Article

Mechanistic Insights into Atom-Economical Bromoalkynylation of Ynamides: 1,3-Alkynyl Migration Explored through ^{13}C Kinetic Isotope Effects, X-ray Photoelectron Spectroscopy, and Density Functional Theory Analysis

Tapas R. Pradhan,[#] Alina Dzhaparova,[#] Gisela A. González-Montiel,[#] Luis Borrego-Castaneda, Eunseok Park, Paul Ha-Yeon Cheong,[*] and Jin Kyoon Park[*]

Cite This: *ACS Catal.* 2025, 15, 21077−21087 Read Online

ACCESS | Metrics & More | Article Recommendations | Supporting Information

ABSTRACT: Difunctionalization of ynamides, whether through an intermolecular approach or in an atom-economical manner, continues to pose a significant challenge. This work presents a simpler method for such unprecedented functionalization through highly regio- and stereoselective bromoalkynylation. The developed strategy, which requires a Pd(II) catalyst and no additive, has a broad scope and high functional-group tolerance and provided access to 50 value-added β-bromo ynenamides. In addition to late-stage functionalization, the synthetic potential of this method was demonstrated through rapid access to previously challenging π-skeletons. A unique 1,3-alkynyl migration, which was enabled by Pd(IV)-bound keteniminium species, offers a platform for the development of atom-economical reactions. Experimental evidence, such as from Hammett plot analysis, X-ray photoelectron spectroscopy studies, and ^{13}C kinetic isotope effect measurements, supported by density functional theory computations enabled a comprehensive understanding of the mechanism.

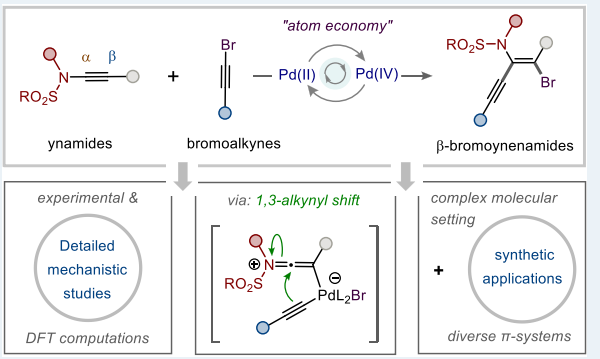

KEYWORDS: *1,3-alkynyl shift, cross-conjugated ynenamides, DFT studies, isotope effect, regioselectivity*

INTRODUCTION

The acquisition of experimental evidence is vital to confidence in science. In chemistry, understanding the mechanisms and factors that influence the rates and selectivities of chemical reactions is essential. Hammett analysis and determination of kinetic isotope effects (KIEs) using the Singleton method have stood out among the array of potent experimental tools available for mechanistic investigations.[1,2] The former technique provides a quantitative measure of the electronic and steric effects of substituents on reaction rates, whereas the latter method offers a complementary approach for elucidating reaction mechanisms.[3] In line with this, carbon-13 isotope distribution provides a sensitive probe for studying the dynamics of carbon-centered reactions with seminal contributions made by Singleton et al.[4] This method enables the determination of very small carbon isotope effects (typically ±0.4−0.7%), providing valuable insight into reaction mechanisms and transition state structures. In this approach, determining intermolecular ^{13}C KIEs at natural abundance depends on kinetic resolution: at high conversion, the unreacted starting material becomes enriched in the slower-reacting isotope (typically ^{13}C), while at low conversion, the product is enriched in the faster-reacting isotope (typically ^{12}C). By analyzing these isotopic distributions, one can deduce the rate-determining step of the reaction, as the magnitude and position of the ^{13}C enrichment reflect the relative bond-making and bond-breaking processes occurring in the transition state.[4]

Since its discovery by Trost et al.,[5] the atom-economical cross-coupling of two different alkynes has been the most frequently employed route to conjugated 1,3-enynes.[6] One particular subset of such coupling reactions is haloalkynylation because it employs a haloalkyne as one coupling partner and brings a higher degree of complexity to these skeletons.[7] Research reported by Jiang et al. in 2010 provided the initial impetus for the search for a Pd(II)-catalyzed haloalkynylation method for an internal alkyne.[8] Notably, the low selectivity (sometimes, a 1:1 ratio) and uncontrolled regioselectivity—either α,β or β,α—for unsymmetrical or functionalized alkynes

Received: August 13, 2025
Revised: November 10, 2025
Accepted: December 2, 2025
Published: December 9, 2025

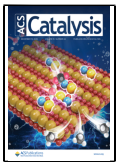

from this pioneering research formed the foundation for the realization of other catalytic variants over the past few years.[9] Although it has a track record of success, a detailed study of its mechanism remains elusive, even though the proposed mechanism appears to be highly feasible.

Ynamides have garnered considerable recognition as valuable components in organic synthesis and exhibit broad applicability across various branches of chemistry. Their remarkable reactivity and versatility make them indispensable for the construction of intricate molecular architectures. In our research, we have envisaged leveraging the potential of these amphiphilic π-systems,[10] in conjunction with haloalkynes, to achieve atom-economical difunctionalization, specifically toward the synthesis of functionalized 1,3-enynes.[10] In the context of ynamide carbofunctionalization,[11] only two nonatom-economical approaches for ynamide difunctionalization for the introduction of alkyne functionalities have been reported.[12,13] One of these is a bimetallic strategy that involves a radical germylzincation employing a superstoichiometric reagent[12] (Scheme 1A), and the other is a monometallic three-component approach (Scheme 1B).[13] Notably, the latter approach, recently introduced by the Sahoo group, involves 1,3-migration through a metal-associated keteniminium intermediate, followed by sequential transmetalation and reductive elimination via Pd(0)/II catalytic cycles. Although these methods have found considerable success in several difunctionalization reactions,[14] they are relatively ineffective for the regioselective installation of an alkyne unit (one example with rr = 2.6:1).[13] In addition, they require the use of a base and multiple reagents. Consequently, the development of atom-economical alternatives for alkynylative difunctionalization is highly desirable. While undertaking the development of the atom-economical difunctionalization of ynamides, we realized that finding an alternative Pd-catalyzed pathway capable of generating an alkyne-$[Pd]^{n+2}$-Br[8,15] complex amenable to reacting with ynamides via a keteniminium species[14] is of utmost importance. For such a concept to be feasible, the challenges of competing α-halogenation (of **1**),[16] homodimerization,[17,18] and careful control of regioisomer formation that could arise from a 1,3-alkynyl shift and a 1,3-bromo shift must be addressed. Moreover, the stereochemical outcomes must be considered with caution, as although no prior reports exist on the coupling of ynamides with internal alkynes, the formation of both *trans*- and *cis*-isomers can undoubtedly be anticipated, as observed in hydroalkynylations (E/Z = 63:37 to >98:2) and Sonogashira reactions (E/Z = 63:37 or 30:70) with α-iodoenamides.[19]

In the context of these challenges and in continuation of our research on halo-functionalized ynenamide synthesis,[20] we present herein our findings on atom-economical Pd(II/IV)-catalyzed bromoalkynylations. As the mechanistic understanding of bromoalkynylation is limited, we elucidated the potential mechanisms through experimental studies, such as Hammett analysis, X-ray photoelectron spectroscopy (XPS) studies, and ^{13}C isotope effect (IE) studies, complemented by density functional theory (DFT) computations. A combination of a wide range of ynamides and bromoalkynes afforded modifiable all-carbon-substituted cross-conjugated ynenamides. The synthetic applicability of this method was demonstrated through the late-stage diversification of complex molecules and valuable synthetic modifications to modularly access complex conjugated π-skeletons that are notoriously difficult to synthesize.

Scheme 1. Precedents Leading to the Discovery of the Present Reaction: (A) Alkynylative Difunctionalization of Ynamide and (B) 1,3-Migration-Enabled Ynamide Difunctionalization

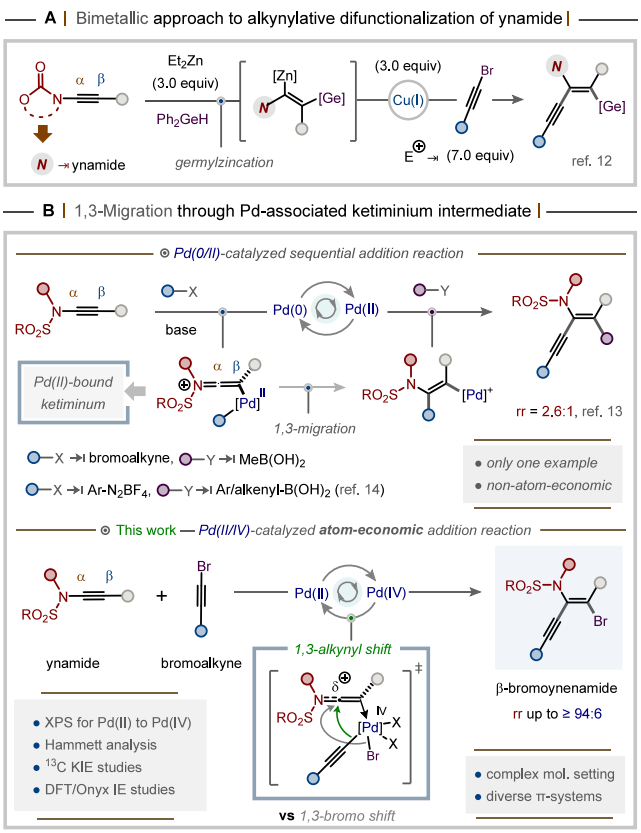

RESULTS AND DISCUSSION

Optimization Overview. Our search for the optimal conditions for the proposed bromoalkynylation of ynamide **1a** began using **2a** under the conditions employed in the previous pioneering studies by Jiang et al.[8,15] Not surprisingly, full conversion of **1a** was observed, producing **3aa** in 43% yield, albeit after 24 h. The low yield is due to the formation of α-bromination product **4a** in 38% yield (see details in the Supporting Information (SI), Table S4). Interestingly, no regio- or stereoisomeric bromoalkynylation products of **3aa** were observed, except in a few cases where minor amounts ($\leq$6%) of the alternative regioisomer (**3′**) formed due to a competing 1,3-bromo shift (vide infra). Encouraged by this result, other parameters such as the catalyst (with or without ligands), additives, solvent, temperature, and concentration were screened toward improving product selectivity (see details in the SI). Notably, additive-free optimal conditions led to desired product **3aa** with perfect stereo- and regioselectivity, which seldom occurs in difunctionalization (Scheme 2).[21]

Scope of the Bromoalkynylation Reaction. Using a set of optimized conditions and with a basic understanding of the factors controlling the regioselectivity, we explored the scope of this transformation by varying the groups at the alkyne terminus. We investigated a series of electronically perturbed aryl-terminated ynamides, which afforded **3ba**–**ia** (Scheme 3A) with perfect regio- and stereoselectivities. We were pleased

https://doi.org/10.1021/acscatal.5c05612
ACS Catal. 2025, 15, 21077−21087

Scheme 2. Standard Conditions for Bromoalkynylation

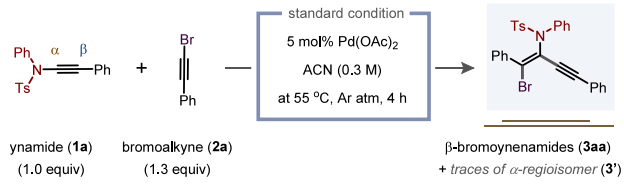

to observe smooth bromoalkynylation for all tested ynamides with similar efficiencies, irrespective of the electronic nature and position of the substituent, although in some cases, ≤6% of the inseparable regioisomer was formed as a result of a competitive 1,3-bromo shift. In addition, the selectivity remained essentially unaffected by either polyaryl or heteroaryl substitution. This was evident as *β*-bromo ynenamides **3ja** and **3ka** were produced in good yields. Notably, this process was similarly effective for both acyclic and cyclic aliphatic ynamides (**3la** and **3ma**). Other aliphatic ynamides with synthetically useful but labile O-protecting groups, such as −OTBS, −OTBDPS, −OBn, and −OBz (**3na**−**qa**), were compatible, generating the corresponding coupling products in reasonable yields (Scheme 3B). However, no traces of the product were formed from the unprotected hydroxyl analogue, presumably because of competitive Pd(II) coordination. Next, we investigated whether ynamide-selective bromoalkynylation could be achieved for conjugated enynamides, wherein both functional groups are prone to react under the standard conditions (Scheme 3C).[15] To our delight, excellent chemoselectivity was observed for both acyclic and cyclic enynamides (**3ra** and **3sa**), further demonstrating the generality of the reaction. Notably, none of the reported haloalkynylation protocols have been employed for such substrates; however, this would allow for the economical construction of valuable unsaturated carbon synthons. However, our attempt to evaluate the chemoselectivity with an alkyne-tethered ynamide proved unsuccessful, as the catalytic condition employed closely resembles that previously known for alkyne.[8]

Additionally, this bromoalkynylation reaction was equally regio- and stereoselective with a wide range of ynamides, irrespective of the electronic and steric biases of the N-protecting groups (Scheme 3D). For example, *N*-aryl substituents can be electron-rich or electron-poor and can be aliphatic groups (methyl, cyclopropyl, and benzyl) (**3ta**−**xa**). Regarding the generality with respect to the *N*-sulfonyl group, smaller and bridged head-fastened ynamides were workable substrates for this transformation, producing other sulfonyl variants of *β*-bromo ynenamides (**3ya**, **3za**, **3Aa**, and **3Ba**). *β*-Bromo ynenamide **3ya** provided a single crystal (CCDC number 2257616), which allowed us to establish its regio- and stereochemistry as well as those of others.

With better insight into the molecular features of ynamide substrates, attention was directed toward understanding the generality of the bromoalkynes. As shown in Scheme 3E, the standard conditions were effective for coupling a range of electronically and sterically different bromoaryl alkynes, albeit with different rates of reaction (**3ab**−**al**). Although no significant steric effects due to the substituents were observed, it is important to note that electronic effects are a substantial factor. The reactivities of the bromoalkynes decreased in the order **2f** > **2a** > **2b** = **2c**. Notably, Pd(II)-reactive competing substrates with halogen substituents, which can undergo further modification, also underwent coupling with exquisite levels of chemoselectivity (no evidence was found for the formation of other products). The cross-coupling of ynamides and bromoalkynes with contrasting electronic substitutions (substituents on the aryl rings) was also feasible (**3cd**). Additionally, a polyaryl bromoalkyne was also a suitable coupling partner, furnishing **3am**. With a highly regioselective and general means to prepare *β*-bromo ynenamides in hand, efforts were next directed toward investigating the synthetic potential of this process in complex molecule modifications, as displayed in Scheme 3F (for eight substrates). Ynamides derived from (L)-menthol, cholesterol, vitamin E, and D-glucose were smoothly converted into the desired products in synthetically acceptable yields with high chemoselectivity (**3Ba**−**Ea**). In addition, the seemingly reactive olefinic bond in the strained ring of a (1*R*)-(−)-nopol-derived ynamide did not have a significant impact on the generation of **3Fa**. An ynamide derived from oleylamine, which is an unsaturated fatty amine, was also suitable for the present cross-coupling reaction (71%, **3Ga**). Considering the apparent mild nature of the standard conditions, we were pleased to find that an estrone-bound bromoalkyne and a chiral-auxiliary-derived ynamide were successfully employed in this transformation (**3al** and **3Hi**, respectively). Although coupling with a terminal ynamide was feasible (albeit with the formation of other stereoisomers), furnishing **3la** in a good yield, the use of silylation and ynamides was unproductive (Scheme 3G). Other limitations of this method include coupling with carbamate-derived electron-withdrawing-group-terminated ynamides, alkyl-terminated alkynyl bromides, and iodoalkynes and chloroalkynes (Scheme 3H, see details in the SI).

Scalability and Further Synthetic Transformations. The scalability of this powerful intermolecular difunctionalization was demonstrated with model substrates **1a** and **2a**, which afforded the product **3aa** in 79% yield on a gram scale (Scheme 4A); however, a slight modification of the standard conditions was required (see details in the SI). The retrosynthesis of fully substituted, stereodefined olefins represents an important challenge in chemical synthesis when considering functionalizable variants. As C−Br bonds are easy to modify, we synthesized synthons with various C−C unsaturations by applying textbook reactions, such as Heck (for **5**), Sonogashira (for **6**), Suzuki (for **7**), and Rosenmund−von Braun (for **8**) reactions. Next, we focused on the development of the *a priori* more demanding intermolecular hydroarylation of ynenamides **7** and **8** (Scheme 4B). Using the conditions from our recent studies on *syn*-hydroarylation of conjugated ynenamides,[22] desired arylated dienamides **9** and **11** were obtained with high regioselectivity and in high yield. This postfunctionalization tactic, which potentially provides access to modular arylated conjugated diene systems, can simplify known strategic disconnections. Furthermore, a Brønsted acid-mediated intramolecular hydroarylation was applied for the synthesis of a substituted *β*-naphthyl amine derivative (**10**), albeit with 6% of a 5-exo-dig cycloisomerization product.

MECHANISTIC INVESTIGATIONS

A Hammett study was conducted using a series of *para*-substituted aryl alkynyl bromides with ynamide **1a** to determine the rates of formation of the *β*-bromo ynenamides (Scheme 5A). Independent rate studies revealed that bromoalkynylation is sensitive to electronic properties; more electron-poor substrates were more reactive. A linear correlation between log([**3aX**]/[**3aa**]) and Hammett constants

https://doi.org/10.1021/acscatal.5c05612
ACS Catal. 2025, 15, 21077−21087

Scheme 3. Study of the Scope of Bromoalkynylation Reaction[a,b,c,d,e,f]: (A) Aryl Group Variation, (B) Alkyl Group Variation, (C) Alkene vs Ynamide Chemoselectivity, (D) N-Substituent Variation, (E) Bromoalkyne Scope, (F) Complex Molecular Setting, (G) Reactivity Study of Other Ynamides, and (H) Limitations

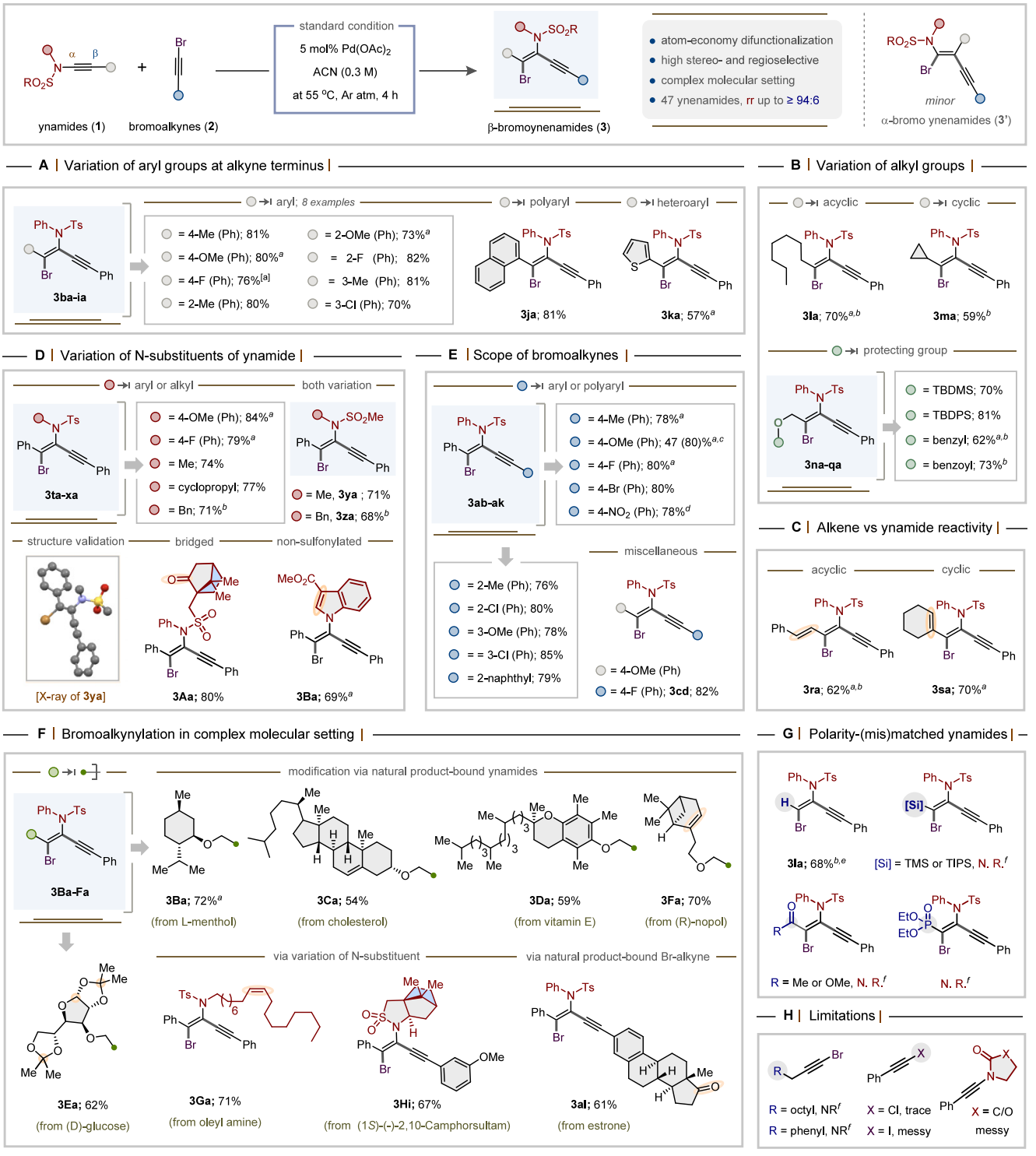

[a]≤6% of other inseparable regioisomer 3′ (see the SI). [b]5−10% of inseparable α/β-bromination byproducts (see the SI). [c]1.5 equiv of **2c** was used. [d]Reaction time was 1 h. [e]7% of another stereoisomer was formed. [f]See details in the SI. N.R. = no reaction.

(s_{para}) with a positive slope (r = +0.82, R^2 = 0.96) was observed, suggesting that a negative charge builds up at the alkyne carbon attached to Pd(IV) in the transition state of the aryl alkynyl bromides (top, Scheme 5A). We further investigated this by conducting ChelpG charges on **I** and **TS-II**, and calculations revealed that the carbons comprising the alkyne in fact increase in negative charge from the intermediate to the transition state. Further details can be found in the SI, Figure S6. DFT analyses for the rate-determining oxidative addition transition states produced

https://doi.org/10.1021/acscatal.5c05612
ACS Catal. 2025, 15, 21077−21087

Scheme 4. Useful Synthetic Applications[a,b,c,d,e]: (A) Scalability and Further Transformations Involving the C−Br Bond of 3aa and (B) Postfunctionalization through Arylation

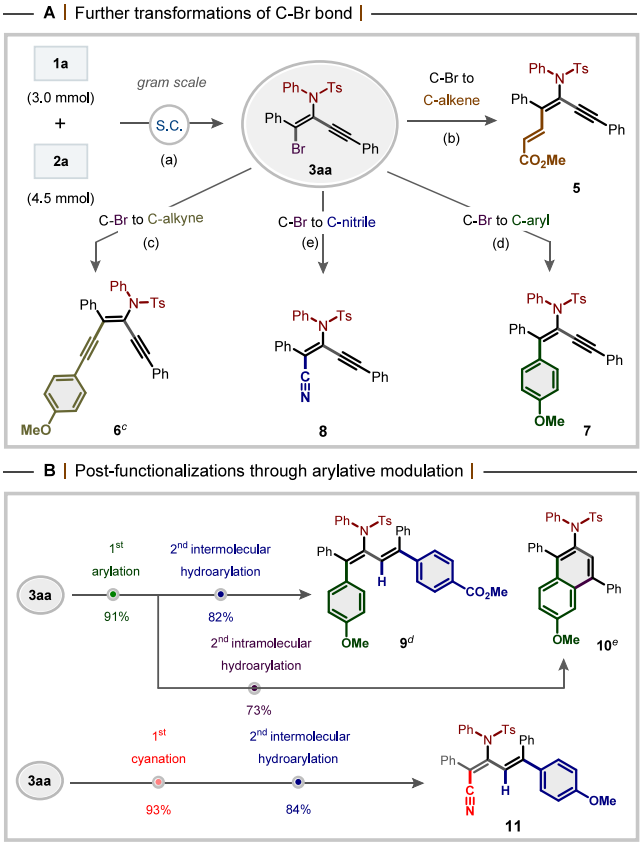

[a]Reagents and conditions: (a) Gram-scale synthesis of **3aa** was performed under standard conditions (S.C.) with slight modification using 5 mmol of **1a** and 7.5 mmol of **2a** (see the SI for details). All further transformations were carried out using 0.1 mmol of **3aa** under the described conditions. (b) Methyl acrylate (2.0 equiv), $Pd(OAc)_2$ (10 mol %), PPh_3 (20 mol %), K_2CO_3 (2.0 equiv), DMF (0.1 M), 90 °C, 8 h, 78%; (c) 1-ethynyl-4-methoxybenzene (1.3 equiv), $Pd(PPh_3)_2Cl_2$ (5 mol %), CuI (10 mol %), Et_3N:THF (1:1, 0.3 M), 50 °C, 6 h, 65%; (d) 4-methoxyphenyl boronic acid (1.5 equiv), $Pd_2(dba)_3$ (2 mol %), SPhos (4 mol %), Cs_2CO_3 (2.0 equiv), THF:H_2O (10:1, 0.5 M), 60 °C, 16 h, 90%; (e) CuCN (3.0 equiv), DMF (0.3 M), 100 °C, 6 h, 92%. [b]For intermolecular postfunctionalization of **7** and **8**: aryl boronic acid (1.2 equiv), $Pd(OAc)_2$ (5 mol %), $PCy_3{\cdot}HBF_4$ (5 mol %), 1,4-dioxane (0.2 M), 60 °C, 3 h, 79%. For intramolecular postfunctionalization of **7**: TfOH (1.1 equiv), DCM (0.3 M), 0 °C to rt, 30 min, 66%. [c]4% of other inseparable stereoisomers. [d]3% of other regio- and stereoisomers. [e]With 6% inseparable stereoisomers possibly resulting from 5-exo-dig cyclization.

similar correlation rates as the experimental results (bottom, Scheme 5A).

Computations showed that a substrate featuring an electron-rich *p*-methoxy substituent forms stable Pd-bromoalkyne complex **I** (ΔG = −9.4 kcal/mol), and then, Pd undergoes a slower oxidative insertion to generate **TS-II** ($\Delta G^{\ddagger}$ = 16.8 kcal/mol), corresponding to an energy barrier of 26.2 kcal/mol. In contrast, a substrate with an electron-poor *p*-nitro substituent forms Pd-bromoalkyne complex **I'** (ΔG = −7.0 kcal/mol), and then, Pd undergoes a faster oxidative insertion to generate **TS-II'** ($\Delta G^{\ddagger}$ = 16.9 kcal/mol), corresponding to an energy barrier of 23.9 kcal/mol. Therefore, the oxidative insertion involving the substrate with the electron-rich *p*-methoxy substituent is slower than that involving the substrate with the electron-poor *p*-nitro substituent by 2.3 kcal/mol, in line with observations that experiments involving electron-rich *p*-substituents are much slower than those involving electron-poor *p*-substituents.

To investigate the involvement of a Pd(II)/Pd(IV) catalytic cycle, we performed XPS analysis to monitor changes in $Pd(OAc)_2$ before and after the reaction, both in the presence and absence of alkynyl bromide, which could potentially act as an oxidant (Scheme 5B).[23] A distinct Pd(IV) signal at 339.1 eV in the Pd $3d_{5/2}$ region was observed exclusively when bromoalkyne was present. Given that the reaction also proceeds—albeit with a lower yield—using Pd(0), we also similarly examined $Pd(dba)_2$ and detected the Pd(IV) signal as well (for more details, see Figure S2). These finding supports the involvement of a Pd(II)/Pd(IV) catalytic cycle in the reaction.

Next, we investigated the ^{13}C IE to gain insight into the mechanism (Scheme 5C). The ^{13}C IEs for this reaction were studied at natural abundance using the NMR methodology by isolating product **3ac** at low conversion instead of analyzing the starting material at higher conversion, as this provides a more comprehensive understanding of the IEs involved. The product obtained at 14% conversion was analyzed using ^{13}C NMR spectroscopy, and the results were compared with those of the product obtained at 100% conversion (see the SI for details). The relative changes in the isotopic composition of each carbon in the ynenamide chain were measured relative to the Ts-methyl carbon as an internal standard, with the assumption that the isotopic fractionation in this carbon was negligible. The optimized values for the IEs were obtained by measuring the changes in the isotopic composition and fractional conversion of the products using the Singleton method[2a] and are presented in Scheme 5C. Interestingly, neither the enamide carbons (C_5 and C_6) nor the alkyne carbons (C_2 and C_3) exhibited substantial ^{13}C IEs, as their values were almost equal to the experimental error of unity. The qualitative interpretation of this observation is that the selectivity-determining step does not involve the synchronous formation of bonds at the ynamide carbons, and this could reflect an inverse IE. Hence, a more quantitative interpretation of the inverse IE was considered with the aid of computational studies to evaluate the expected IE and the differences between the different mechanistic scenarios (vide infra, Figure 3).

With the results of the Hammett study and the ^{13}C IEs in hand, our attention shifted toward gaining better insight into the operative mechanism. A plausible key for the selectivity is 1,3-alkynyl migration via the initially proposed Pd(II/IV) catalytic cycle.[8] That is, in this process, the oxidative addition of the alkynyl bromide produces electrophilic complex **III**, which can regioselectively direct the alkyne unit to the *α*-position of the ynamide via a high-valence Pd(IV)-bound alkyne intermediate.[24]

Based on the above experimental results, we explored the mechanism of the formation of *β*-bromo ynenamide **3ac** using DFT with PBE-D3BJ/LANL2DZ(Pd) and 6-31G* for all other atoms and with SMD(CH_3CN) solvation corrections at 55 °C as implemented in Gaussian 16.[25,26,27] Single-point calculations were performed at the PBE-D3BJ/def2-TZVP level of theory, with the same solvation corrections. Exhaustive conformational searches were conducted on structures, and all low-energy conformations were refined by DFT.

https://doi.org/10.1021/acscatal.5c05612
ACS Catal. 2025, 15, 21077−21087

Scheme 5. Experimental Mechanistic Studies Supported by DFT: (A) Hammett Analysis, (B) XPS Analysis, and (C) ^{13}C KIE Studies

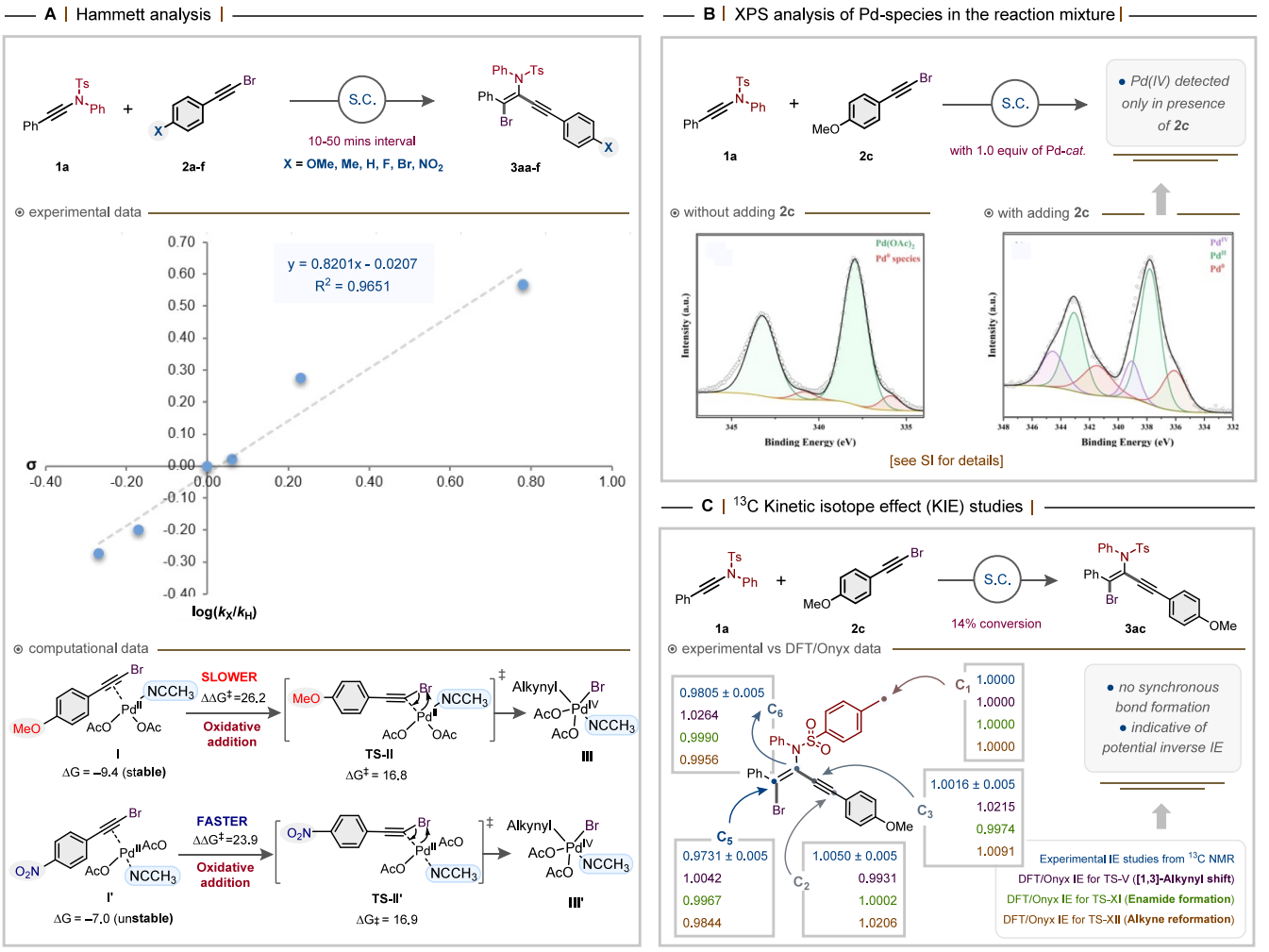

Alternative reaction pathways were also considered by DFT (Figures S7 and S8). The proposed catalytic cycle is shown in Scheme 6, and the complete reaction coordinate diagram and energies are listed in Figure 1.

The catalytic cycle for the formation of product **3ac** begins with the coordination of bromoalkyne **2c** and CH_3CN to $Pd(OAc)_2$ to give Pd(II)-alkyne-CH_3CN complex **I**, the resting state of the catalytic cycle (ΔG = 0.0 kcal/mol) (see the SI, Figure S9). Oxidative insertion of Pd into the C−Br σ bond of **2c**, which is the rate-determining step in this reaction, affords Pd(IV) complex **III** (Scheme 5A, vide supra, and Figure S4). It is worth mentioning that the initially proposed *cis* insertion pathway[8] is not possible based on the following observations: (1) complete selectivity toward the α-alkynylated regioisomer was shown for both aryl and alkyl ynamides, in contrast to the uncontrolled selectivity observed by Jiang et al., and (2) a chelation-prone oxazolidinone-based ynamide produced a mixture of isomers (vide supra), which is consistent with the 1,3-aryl migration process enabled by a keteniminium species.[13] Instead, the bromoalkynylation of Pd(IV) complex **III** with ynamide **1a** (ΔG = 21.3 kcal/mol) starts with an ynamide exchange and the release of CH_3CN to give complex **IV** (ΔG = 15.9 kcal/mol). Bromoalkynylation occurs via the acetate-assisted stepwise alkynyl migration,

Scheme 6. Proposed Catalytic Cycle for the Pd(II)-Catalyzed Bromoalkynylation of Ynamide 1a

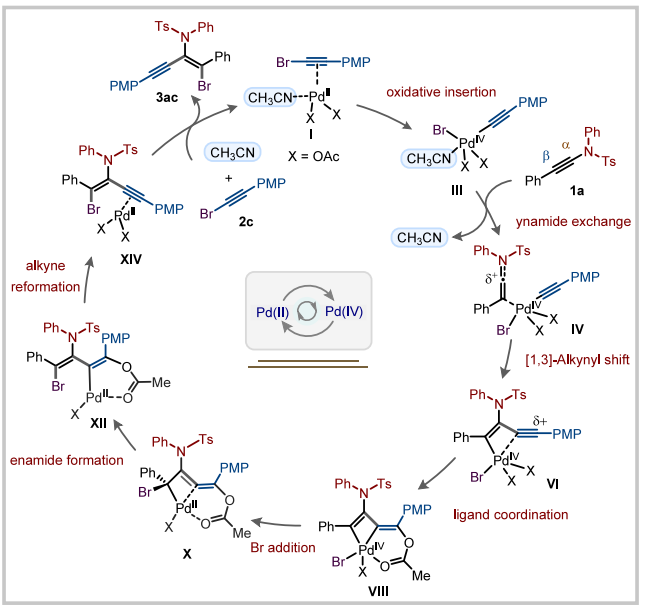

https://doi.org/10.1021/acscatal.5c05612
ACS Catal. 2025, 15, 21077−21087

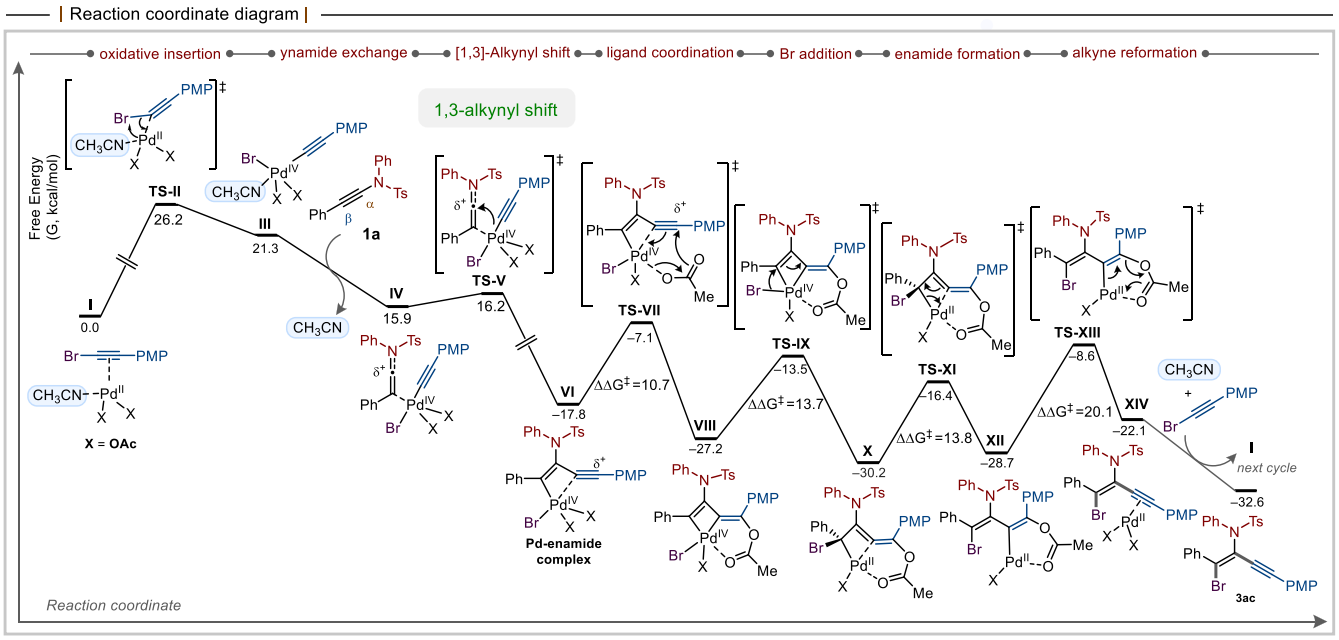

Figure 1. Complete mechanism and quantum mechanically computed energies for the formation of *β*-bromo ynenamide **3ac**. Energies were calculated with PBE-D3BJ/LANL2DZ(Pd) and 6-31G* for all other atoms and with SMD(CH_3CN) solvation corrections at 55 °C. Energies were further refined with single-point calculations at the PBE-D3BJ/def2-TZVP level of theory with the same solvation corrections.

which controls whether the 1,3-alkynyl shift or 1,3-bromo shift occurs (Figure 2).

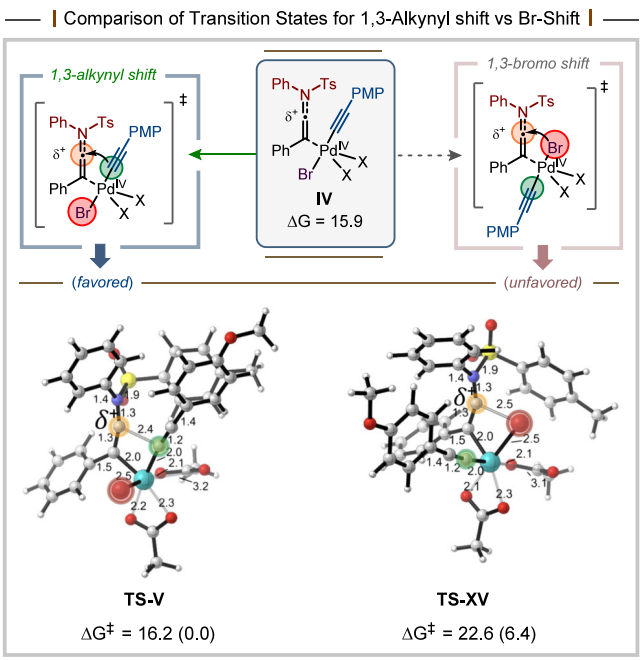

Figure 2. Computed transition structures and energies for the favored [1,3]-alkynyl shift, **TS-V** (left) versus the unfavored [1,3]-bromo shift, **TS-XV** (right).

The favored pathway occurs via a facile [1,3]-alkynyl shift to the ynamide *α*-carbon (**TS-V**, $\Delta G^{\ddagger}$ = 16.2 kcal/mol). The unfavored pathway occurs via a [1,3]-bromo shift (**TS-XV**, $\Delta G^{\ddagger}$ = 22.6 kcal/mol), which is 6.4 kcal/mol higher in energy. The alkynyl shift is strongly preferred over the bromo shift because the former leads to conjugation between the ynamide and alkynyl groups and the formation of a stabilized benzylic partial carbocation. In contrast, the disfavored bromo shift leads to a strained bridged halogen in a four-membered ring complex with Pd. Hence, the favored [1,3]-alkynyl shift leads to Pd-enamide complex **VI** (ΔG = −17.8 kcal/mol). The observed syn-selectivity in the bromoalkynylation is readily rationalized by an inner-sphere sequence that locks both new bonds to the same face of the alkyne before C−Pd bond cleavage. From Pd-enamide complex **VI**, acetate ligand coordination at the benzylic carbon of the alkyne (**TS-VII**, $\Delta G^{\ddagger}$ = −7.1 kcal/mol) generates 4,6-bicyclic Pd(IV) complex **VIII** (ΔG = −27.2 kcal/mol). The analogous stepwise process where the Pd−C bond formation and acetate ligand coordination occur sequentially was disfavored by ∼2 kcal/mol (see the SI, Figure S8). The addition of Br at the ynamide *β*-carbon (**TS-IX**, $\Delta G^{\ddagger}$ = −13.5 kcal/mol) gives 4,6-bicyclic Pd(II) complex **X** (ΔG = −30.2 kcal/mol). In this rigid bicyclic geometry, the ynamide *π*-system, the Pd center, and the incoming bromo group are held in a single coordination environment, so addition of Br to the ynamide *β*-carbon (**TS-IX**) occurs from the same face as the alkynyl/Pd fragment. The resulting complex **X** undergoes Pd−C_β bond cleavage (**TS-XI**, $\Delta G^{\ddagger}$ = −16.4 kcal/mol) only after bromination, via the formation of enamide complex **XII** (ΔG = −28.7 kcal/mol) while conserving the relative stereochemistry. Thus, *syn* delivery of Br and the alkynyl substituent is imposed by the bicyclic, inner-sphere coordination geometry prior to any Pd−C bond scission and is consistent with the low barriers and strongly exergonic formation of the bicyclic intermediate **X**. Liberation of the acetate from the benzylic carbon regenerates the alkyne (**TS-XIII**, $\Delta G^{\ddagger}$ = −8.6 kcal/mol) and gives the Pd-product complex **XIV** (ΔG = −22.1 kcal/mol). Finally, a second bromoalkyne **2c** inclusion and CH_3CN incorporation into **XIV** release the major product, *β*-bromo ynenamide **3ac**, and regenerate complex **I** for the next catalytic cycle.

For a more precise interpretation of the experimental ^{13}C IE measurements (cf. Scheme 5C), the IE values were calculated by using Onyx from DFT structures to evaluate the proposed

https://doi.org/10.1021/acscatal.5c05612
ACS Catal. 2025, 15, 21077−21087

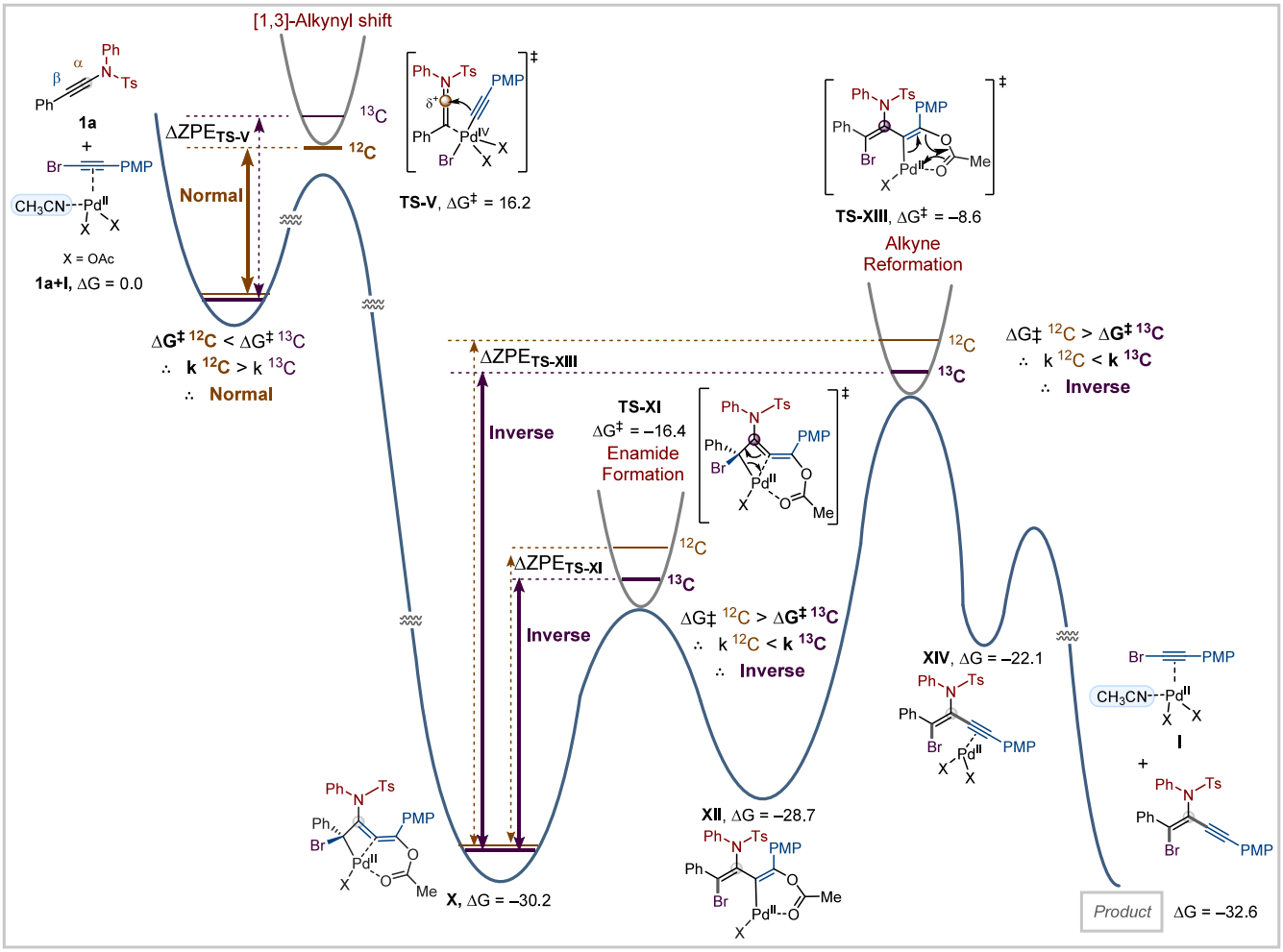

Figure 3. Explanation for the ^{13}C inverse kinetic isotope effect (IKIE) value of the relevant enamide carbon from DFT/Onyx IE studies. Energies were calculated with PBE-D3BJ/LANL2DZ(Pd) and 6-31G* for all other atoms and with SMD(CH_3CN) solvation corrections at 55 °C. Energies were further refined with single-point calculations at the PBE-D3BJ/def2-TZVP level of theory with the same solvation corrections.

mechanism. This method has previously been used to study the equilibrium IE of supramolecular complexes[28] (Figure 3). The relative changes in the isotopic composition of each carbon in the ynenamide chain were also measured relative to that of the Ts-methyl carbon as an internal standard. First, the IE values for the [1,3]-alkynyl shift were computed. The DFT Onyx IE studies gave an expected normal IE value for enamide carbon C_6 (>1.0, highlighted in orange), where $\Delta G^{\ddagger\,12}C < \Delta G^{\ddagger\,13}C$, meaning $k\ ^{12}C > k\ ^{13}C$, and therefore, the IE is normal. Then, we computed the relevant IE values for the conversion of resting-state 4,6-bicyclic Pd(II) complex **X** to alkyne formation transition state **TS-XIII**. With an energy barrier of 21.6 kcal/mol, this is the highest-energy transition state following the addition of ynamide. The DFT Onyx IE studies also revealed an inverse IE for enamide carbon C_6 (<1.0, highlighted purple), where $\Delta G^{\ddagger\,12}C > \Delta G^{\ddagger\,13}C$, meaning $k\ ^{12}C < k\ ^{13}C$, and therefore, there is an inverse kinetic IE (IKIE). These values differ from the observed ^{13}C NMR IE values by $\Delta G = -0.01$ kcal/mol. We rationalized that the IKIE value is not the result of a single concerted reductive elimination step, which would yield a normal kinetic IE (NKIE), but rather a two-step process.[29] From the metallacyclobutene in **X**, the enamide is formed (**X** to **TS-XI**, 13.8 kcal/mol), breaking the C_5−Pd bond to give conjugated diene **XII**. Then, the C_2−O bond breaks, reforming the alkyne of the ynenamide (**XII** to **TS-XIII**, 20.1 kcal/mol) and restoring the coordination between the OAc ligand and palladium. Hence, C_5−Pd bond cleavage is not the rate-determining step. Taken together, these results suggest that the experimentally observed IKIE arises from an irreversible stepwise elimination.

CONCLUSIONS

This work presents yet another remarkable example of how the regio- and stereoselectivity of bromoalkynylation can be completely regulated by using N-conjugated ynamides. To the best of our knowledge, this is the first example of an atom-economical Pd-catalyzed intermolecular alkynylative difunctionalization of ynamides. 1,3-Alkynyl migration, a hitherto unknown phenomenon in (halo)alkynylation, governs the regioselectivity. These additive-free reaction conditions provided a general and highly selective protocol, as proven by granting access to 50 fully substituted functionalized ynenamides and enabling late-stage functionalization. This simple but modular tactic for the construction of synthetically versatile unsaturated carbon skeletons reflects the synthetic potential of the developed method. A fully understood catalytic

https://doi.org/10.1021/acscatal.5c05612
ACS Catal. 2025, 15, 21077−21087

cycle that involves the rate-determining oxidative addition of a bromoalkyne followed by a 1,3-alkynyl shift was proposed. This proposal was supported by experimental and computational ^{13}C IE studies and Hammett analysis. Furthermore, XPS analysis supported a more favorable and chemoselective Pd(II) to Pd(IV) pathway as a plausible reaction mechanism. The unorthodox reactivity pattern exhibited by bromoalkynes for ynamides may serve as a general platform for other C−C π-systems.

METHODS

General Procedure for Bromoalkynylation of Ynamides. A screw-capped 7 mL vial equipped with a Teflon-coated magnetic stir bar was added with the appropriate ynamides **1** (0.2 mmol) and bromoalkynes **2** (0.26 mmol). The vial was sealed with a screw-top septum cap and then evacuated and backfilled with argon three times. Under a positive pressure of argon (maintained by an argon balloon), anhydrous acetonitrile (0.6 mL) was added. 5 mol % $Pd(OAc)_2$ (2.24 mg) was added to this solution in one portion. The reaction mixture was allowed to stir at 55 °C by means of a preheated heating block for 6 h. After complete consumption of the starting ynamides **1**, as indicated by TLC, the solvent was removed under reduced pressure to yield a dark-brown residue. Purification of this residue by silica gel column chromatography, using petroleum ether and ethyl acetate as the eluent, afforded the corresponding bromoalkynylation products (**3**). Please refer to the Supporting Information for details.

ASSOCIATED CONTENT

Supporting Information

The Supporting Information is available free of charge at https://pubs.acs.org/doi/10.1021/acscatal.5c05612.

Experimental procedures, compound characterization data, and NMR spectra (PDF)

Accession Codes

CCDC 2257616 (**3ya**) contains the supplementary crystallographic data for this paper. These data can be obtained free of charge via www.ccdc.cam.ac.uk/data_request/cif, or by emailing data_request@ccdc.cam.ac.uk, or by contacting The Cambridge Crystallographic Data Centre, 12 Union Road, Cambridge CB2 1EZ, UK; fax: +44 1223 336033.

AUTHOR INFORMATION

Corresponding Authors

Paul Ha-Yeon Cheong − *Department of Chemistry, Oregon State University, Corvallis, Oregon 97331, United States;* orcid.org/0000-0001-6705-2962; Email: paulc@science.oregonstate.edu

Jin Kyoon Park − *Department of Chemistry Education, Seoul National University, Seoul 08826, Republic of Korea;* orcid.org/0000-0001-6768-2788; Email: pjkyoon@snu.ac.kr

Authors

Tapas R. Pradhan − *Department of Chemistry Education, Seoul National University, Seoul 08826, Republic of Korea;* orcid.org/0000-0003-1480-7799

Alina Dzhaparova − *Department of Chemistry and Chemistry Institute for Functional Materials, Pusan National University, Busan 46241, Republic of Korea*

Gisela A. González-Montiel − *Department of Chemistry, Oregon State University, Corvallis, Oregon 97331, United States*

Luis Borrego-Castaneda − *Department of Chemistry, Oregon State University, Corvallis, Oregon 97331, United States*

Eunseok Park − *Bruker Biospin Korea, Seoul 13493, Republic of Korea*

Complete contact information is available at: https://pubs.acs.org/10.1021/acscatal.5c05612

Author Contributions

#T.R.P., A.D., and G.A.G.-M. contributed equally to this work. All authors have approved the final version of the manuscript.

Notes

The authors declare no competing financial interest.

ACKNOWLEDGMENTS

This study was supported financially by the National Research Foundation of Korea (NRF) (RS-2024-00340803 and RS-2025-02215028) and the Samsung Science & Technology Foundation (SSTF-BA190113746). P.H.-Y.C. is the Bert and Emelyn Christensen professor at OSU and gratefully acknowledges financial support from the National Science Foundation (NSF, CHE-1352663).

REFERENCES

(1) (a) Hammett, L. P. Some Relations between Reaction Rates and Equilibrium Constants. *Chem. Rev.* **1935**, *17*, 125. (b) Hammett, L. P.*Physical Organic Chemistry*; McGraw-Hill Book Co.: London, 1970.
(2) (a) Singleton, D. A.; Thomas, A. A. High-Precision Simultaneous Determination of Multiple Small Kinetic Isotope Effects at Natural Abundance. *J. Am. Chem. Soc.* **1995**, *117*, 9357. (b) Meyer, M. P. Chapter 2 - New Applications of Isotope Effects in the Determination of Organic Reaction Mechanisms. *Adv. Phys. Org. Chem.* **2012**, *46*, 57.
(3) (a) Singleton, D. A.; Hang, C.; Szymanski, M. J.; Meyer, M. P.; Leach, A. G.; Kuwata, K. T.; Chen, J. S.; Greer, A.; Foote, C. S.; Houk, K. N. Mechanism of Ene Reactions of Singlet Oxygen. A Two-Step No-Intermediate Mechanism. *J. Am. Chem. Soc.* **2003**, *125*, 1319. (b) Bandar, J. S.; Sauer, G. S.; Wulff, W. D.; Lambert, T. H.; Vetticatt, M. J. Transition State Analysis of Enantioselective Brønsted Base Catalysis by Chiral Cyclopropenimines. *J. Am. Chem. Soc.* **2014**, *136*, 10700. (c) Crich, D. *Acc. Chem. Res.* **2010**, *43*, 1144. (d) Ryan, S. J.; Candish, L.; Lupton, D. W. N-Heterocyclic Carbene-Catalyzed (4 + 2) Cycloaddition/Decarboxylation of Silyl Dienol Ethers with α,β-Unsaturated Acid Fluorides. *J. Am. Chem. Soc.* **2011**, *133*, 4694. (e) Dahlen, A.; Hilmersson, G. Mechanistic Study of the SmI_2/H_2O/Amine-Mediated Reduction of Alkyl Halides: Amine Base Strength (pK_{BH+}) Dependent Rate. *J. Am. Chem. Soc.* **2005**, *127*, 8340. (f) Yoshikai, N.; Nakamura, E. Mechanism of Substitution Reaction on sp^2-Carbon Center with Lithium Organocuprate. *J. Am. Chem. Soc.* **2004**, *126*, 12264.
(4) (a) Singleton, D. A.; Wang, Y.; Yang, H. W.; Romo, D. Mechanism and Origin of Stereoselectivity in Lewis Acid Catalyzed [2 + 2] Cycloadditions of Ketenes with Aldehydes. *Angew. Chem., Int. Ed.* **2002**, *41*, 1572. (b) Ashley, M. A.; Hirschi, J. S.; Izzo, J. A.; Vetticatt, M. J. Isotope Effects Reveal the Mechanism of Enamine Formation in L-Proline-Catalyzed α-Amination of Aldehydes. *J. Am. Chem. Soc.* **2016**, *138*, 1756. (c) Izzo, J. A.; Poulsen, P. H.; Intrator, J. A.; Jørgensen, K. A.; Vetticatt, M. J. Isotope Effects Reveal an Alternative Mechanism for "Iminium-Ion" Catalysis. *J. Am. Chem. Soc.* **2018**, *140*, 8396. (d) Mallojjala, S. C.; Nyagilo, V. O.; Corio, S. A.; Adili, A.; Dagar, A.; Loyer, K. A.; Seidel, D.; Hirschi, J. S. Probing the Free Energy Landscape of Organophotoredox-Catalyzed Anti-Markovnikov Hydrofunctionalization of Alkenes. *J. Am. Chem. Soc.* **2022**, *144*, 17692. (e) DelMonte, A. J.; Haller, J.; Houk, K. N.; Sharpless, K. B.; Singleton, D. A.; Strassner, T.; Thomas, A. A. Experimental and

Theoretical Kinetic Isotope Effects for Asymmetric Dihydroxylation. Evidence Supporting a Rate-Limiting "(3 + 2)" Cycloaddition. *J. Am. Chem. Soc.* **1997**, *119*, 9907−9908.
(5) (a) Trost, B. M.; Chan, C.; Rühter, G. Metal-Mediated Approach to Enynes. *J. Am. Chem. Soc.* **1987**, *109*, 3486. (b) Trost, B. M.; Sorum, M. T.; Chan, C.; Harms, A. E.; Rühter, G. Palladium-Catalyzed Additions of Terminal Alkynes to Acceptor Alkynes. *J. Am. Chem. Soc.* **1997**, *119*, 698.
(6) For reviews, see: (a) Trost, B. M.; Masters, J. T. Transition metal-catalyzed couplings of alkynes to 1,3-enynes: modern methods and synthetic applications. *Chem. Soc. Rev.* **2016**, *45*, 2212. Representative articles: (b) Weber, S.; Veiros, L. F.; Kirchner, K. Selective Manganese-Catalyzed Dimerization and Cross-Coupling of Terminal Alkynes. *ACS Catal.* **2021**, *11*, 6474. (c) Liang, Q.; Sheng, K.; Salmon, A.; Zhou, V. Y.; Song, D. Active Iron(II) Catalysts toward *gem*-Specific Dimerization of Terminal Alkynes. *ACS Catal.* **2019**, *9*, 810. (d) Chen, J.-F.; Li, C. Cobalt-Catalyzed gem-Cross-Dimerization of Terminal Alkynes. *ACS Catal.* **2020**, *10*, 3881. (e) Lauer, M. G.; Headford, B. R.; Gobble, O. M.; Weyhaupt, M. B.; Gerlach, D. L.; Zeller, M.; Shaughnessy, K. H. A Trialkylphosphine-Derived Palladacycle as a Catalyst in the Selective Cross-Dimerization of Terminal Arylacetylenes with Terminal Propargyl Alcohols and Amides. *ACS Catal.* **2016**, *6*, 5834. (f) Liu, M.; Tang, T.; Apolinar, O.; Matsuura, R.; Busacca, C. A.; Qu, B.; Fandrick, D. R.; Zatolochnaya, O. V.; Senanayake, C. H.; Song, J. J.; Engle, K. M. Atom-Economical Cross-Coupling of Internal and Terminal Alkynes to Access 1,3-Enynes. *J. Am. Chem. Soc.* **2021**, *143*, 3881.
(7) For reviews on halolakynylation, see: (a) Wu, W.; Jiang, H. Haloalkynes: A Powerful and Versatile Building Block in Organic Synthesis. *Acc. Chem. Res.* **2014**, *47*, 2483. (b) Kreuzahler, M.; Haberhauer, G. Metal-Catalyzed Haloalkynylation Reactions. *Chem.—Eur. J.* **2022**, *28*, No. e202103046.
(8) Li, Y.; Liu, X.; Jiang, H.; Feng, Z. Expedient Synthesis of Functionalized Conjugated Enynes: Palladium-Catalyzed Bromoalkynylation of Alkynes. *Angew. Chem., Int. Ed.* **2010**, *49*, 3338.
(9) (a) Wada, T.; Iwasaki, M.; Kondoh, A.; Yorimitsu, H.; Oshima, K. Palladium-Catalyzed Addition of Silyl-Substituted Chloroalkynes to Terminal Alkynes. *Chem. - Eur. J.* **2010**, *16*, 10671. (b) Mader, S.; Molinari, L.; Rudolph, M.; Rominger, F.; Hashmi, A. S. K. Dual Gold-Catalyzed Head-to-Tail Coupling of Iodoalkynes. *Chem.—Eur. J.* **2015**, *21*, 3910. (c) Kreuzahler, M.; Daniels, A.; Wölper, C.; Haberhauer, G. 1,3-Chlorine Shift to a Vinyl Cation: A Combined Experimental and Theoretical Investigation of the *E*-Selective Gold(I)-Catalyzed Dimerization of Chloroacetylenes. *J. Am. Chem. Soc.* **2019**, *141*, 1337. (d) Kreuzahler, M.; Haberhauer, G. Gold(I)-Catalyzed Haloalkynylation of Aryl Alkynes: Two Pathways. *One Goal. Angew. Chem. Int. Ed.* **2020**, *59*, 9433. (e) García-Fernández, P. D.; Iglesias-Sigüenza, J.; Rivero-Jerez, P. S.; Díez, E.; Gómez-Bengoa, E.; Fernández, R.; Lassaletta, J. M. Au^{I}-Catalyzed Hydroalkynylation of Haloalkynes. *J. Am. Chem. Soc.* **2020**, *142*, 16082. (f) Barsu, N.; Leutzsch, M.; Fürstner, A. Ruthenium-Catalyzed *trans*-Hydroalkynylation and *trans*-Chloroalkynylation of Internal Alkynes. *J. Am. Chem. Soc.* **2020**, *142*, 18746.
(10) (a) DeKorver, K. A.; Li, H.; Lohse, A. G.; Hayashi, R.; Lu, Z.; Zhang, Y.; Hsung, R. P. Ynamides: A Modern Functional Group for the New Millennium. *Chem. Rev.* **2010**, *110*, 5064. (b) Evano, G.; Coste, A.; Jouvin, K. Ynamides: Versatile Tools in Organic Synthesis. *Angew. Chem., Int. Ed.* **2010**, *49*, 2840. (c) Wang, X. N.; Yeom, H. S.; Fang, L. C.; He, S.; Ma, Z. X.; Kedrowski, B. L.; Hsung, R. P. Ynamides in Ring Forming Transformations. *Acc. Chem. Res.* **2014**, *47*, 560. (d) Prabagar, B.; Ghosh, N.; Sahoo, A. K. Cyclization and Cycloisomerization of π-Tethered Ynamides: An Expedient Synthetic Method to Construct Carbo- and Heterocycles. *Synlett* **2017**, *28*, 2539. (e) Pan, F.; Shu, C.; Ye, L.-W. Recent progress towards gold-catalyzed synthesis of N-containing tricyclic compounds based on ynamides. *Org. Biomol. Chem.* **2016**, *14*, 9456.
(11) (a) Greenaway, R. L.; Campbell, C. D.; Holton, O. T.; Russell, C. A.; Anderson, E. A. Palladium-Catalyzed Cascade Cyclization of Ynamides to Azabicycles. *Chem.—Eur. J.* **2011**, *17*, 14366. (b) Saito, N.; Saito, K.; Sato, H.; Sato, Y. Regio- and Stereoselective Synthesis of Tri- and Tetrasubstituted Enamides *via* Palladium-Catalyzed Silaboration of Ynamides. *Adv. Synth. Catal.* **2013**, *355*, 853. (c) Campbell, C. D.; Greenaway, R. L.; Holton, O. T.; Walker, P. R.; Chapman, H. A.; Russell, C. A.; Carr, G.; Thomson, A. L.; Anderson, E. A. Ynamide Carbopalladation: A Flexible Route to Mono-, Bi- and Tricyclic Azacycles. *Chem.—Eur. J.* **2015**, *21*, 12627. (d) Dutta, S.; Mallick, R. K.; Sahoo, A. K. Regioselective Difunctionalization and Annulation of Ynamide. *Angew. Chem., Int. Ed.* **2023**, *62*, No. e202300816.
(12) de la Vega-Hernández, K.; Romain, E.; Coffinet, A.; Bijouard, K.; Gontard, G.; Chemla, F.; Ferreira, F.; Jackowski, O.; Perez-Luna, A. Radical Germylzincation of α-Heteroatom-Substituted Alkynes. *J. Am. Chem. Soc.* **2018**, *140*, 17632.
(13) Dutta, S.; Sahoo, A. K. Three Component *syn*-1,2-Arylmethylation of Internal Alkynes. *Angew. Chem., Int. Ed.* **2023**, *62*, No. e202300610.
(14) (a) Dutta, S.; Yang, S.; Vanjari, R.; Mallick, R. K.; Gandon, V.; Sahoo, A. K. Keteniminium-Driven Umpolung Difunctionalization of Ynamides. *Angew. Chem., Int. Ed.* **2020**, *59*, 10785. (b) Vanjari, R.; Dutta, S.; Yang, S.; Gandon, V.; Sahoo, A. K. Palladium-Catalyzed Regioselective Arylalkenylation of Ynamides. *Org. Lett.* **2022**, *24*, 1524.
(15) Li, Y.; Liu, X.; Jiang, H.; Liu, B.; Chen, Z.; Zhou, P. Palladium-Catalyzed Bromoalkynylation of C−C Double Bonds: Ring-Structure-Dependent Synthesis of 7-Alkynyl Norbornanes and Cyclobutenyl Halides. *Angew. Chem., Int. Ed.* **2011**, *50*, 6341.
(16) For articles on α-halogenation with *in situ* generated halide ions: (a) Cao, W.; Chen, P.; Wang, L.; Wen, H.; Liu, Y.; Wang, W.; Tang, Y. A Highly Regio- and Stereoselective Syntheses of α-Halo Enamides, Vinyl Thioethers, and Vinyl Ethers with Aqueous Hydrogen Halide in Two-Phase Systems. *Org. Lett.* **2018**, *20*, 4507. (b) Wen, H.; Yan, W.; Chen, P.; Li, Y.; Tang, Y. Catalyst-Free [4 + 2] Cycloaddition of Ynamides with 2-Halomethyl Phenols To Construct 2-Amino-4H-Chromenes and α-Halo Enamides Simultaneously. *J. Org. Chem.* **2020**, *85*, 12870.
(17) For homodimerization of ynamides: Kramer, S.; Odabachian, Y.; Overgaard, J.; Rottländer, M.; Gagosz, F.; Skrydstrup, T. Taking Advantage of the Ambivalent Reactivity of Ynamides in Gold Catalysis: A Rare Case of Alkyne Dimerization. *Angew. Chem., Int. Ed.* **2011**, *50*, 5090.
(18) (a) ref. 9b and 9c of this paper. (b) Damle, S. V.; Seomoon, D.; Lee, P. H. Palladium-Catalyzed Homocoupling Reaction of 1-Iodoalkynes: A Simple and Efficient Synthesis of Symmetrical 1,3-Diynes. *J. Org. Chem.* **2003**, *68*, 7085.
(19) (a) Liu, G.; Kong, W.; Che, J.; Zhu, G. Palladium-Catalyzed Cross Addition of Terminal Alkynes to Aryl Ynamides: An Unusual *trans*-Hydroalkynylation Reaction. *Adv. Synth. Catal.* **2014**, *356*, 3314. (b) Dwivedi, V.; Babu, M. H.; Kant, R.; Reddy, M. S. *N*-Substitution dependent stereoselectivity switch in palladium catalyzed hydroalkynylation of ynamides: a regio and stereoselective synthesis of ynenamides. *Chem. Commun.* **2015**, *51*, 14996. (c) Prabagar, B.; Nayak, S.; Mallick, R. K.; Prasad, R.; Sahoo, A. K. Triphenylphosphine promoted regio and stereoselective α-halogenation of ynamides. *Org. Chem. Front.* **2016**, *3*, 110. (d) Zeng, Z.; Lu, Z.; Hammond, G. B.; Xu, B. Metal-free, Regio-, and Stereo-Controlled Hydrochlorination and Hydrobromination of Ynones and Ynamides. *J. Org. Chem.* **2017**, *82*, 13179. For a recent example employing the use of gold catalysis in acyloxyalkynylation of ynamides following an altered regio- and stereochemistry, see: (e) Liu, Y.; Dietl, M. C.; Han, C.; Rudolph, M.; Rominger, F.; Krämer, P.; Hashimi, A. S. K. Synthesis of Amide Enol 2-Iodobenzoates by the Regio- and Stereoselective Gold-Catalyzed Acyloxyalkynylation of Ynamides with Hypervalent Iodine Reagents. *Org. Lett.* **2022**, *24*, 7101.
(20) (a) Pradhan, T. R.; Paudel, M.; Harper, J. L.; Cheong, P. H.-Y.; Park, J. K. Characterization and Utilization of the Elusive α,β-Unsaturated N-Tosyliminium: The Synthesis of Highly Functionalizable Skipped Halo Enynes. *Org. Lett.* **2021**, *23*, 1427. (b) Lee, H. E.; Pradhan, T. R.; Kim, Y.; Park, J. K. Stable Vinylogous Aminal Salt as a

https://doi.org/10.1021/acscatal.5c05612
ACS Catal. 2025, 15, 21077−21087

Reactive Synthon for the Synthesis of Homologated β-Fluoroenamides. *Org. Lett.* **2025**, *27*, 7342−7348.
(21) To examine the possibility that the reaction might be promoted by visible light as suggested by the reviewer, the reaction was conducted under dark conditions. The desired product **3aa** was obtained in 84% yield, indicating that light does not have a significant effect on this transformation.
(22) A study on hydroarylation of this kind of ynenamide with complete details will be reported in due course.
(23) Kim, K.; Jung, Y.; Lee, S.; Kim, M.; Shin, D.; Byun, H.; Cho, S. J.; Song, H.; Kim, H. Directed C−H Activation and Tandem Cross-Coupling Reactions Using Palladium Nanocatalysts with Controlled Oxidation. *Angew. Chem., Int. Ed.* **2017**, *56*, 6952.
(24) For an example on atom-economy difunctionalization of ynamides involving Pd(II)/Pd(IV) catalysis, see: Hansjacob, P.; Leroux, F. R.; Gandon, V.; Donnard, M. Palladium-Catalyzed Silylcyanation of Ynamides: Regio- and Stereoselective Access to Tetrasubstituted 3-Silyl-2-Aminoacrylonitriles. *Angew. Chem., Int. Ed.* **2022**, *61*, No. e202200204.
(25) For PBE reference: (a) Perdew, J. P.; Burke, K.; Ernzerhof, M. Generalized Gradient Approximation Made Simple. *Phys. Rev. Lett.* **1996**, *77*, 3865. (b) Perdew, J. P.; Burke, K.; Ernzerhof, M. K^+ Emission in Symmetric Heavy Ion Reactions at Subthreshold Energies. *Phys. Rev. Lett.* **1997**, *78*, 1396. For D3BJ reference: (c) Grimme, S.; Ehrlich, S.; Goerigk, L. Effect of the damping function in dispersion corrected density functional theory. *J. Comput. Chem.* **2011**, *32*, 1456. For LANL2DZ reference: (d) Hay, P. J.; Wadt, W. R. Ab Initio effective core potentials for molecular calculations. Potentials for the transition metal atoms Sc to Hg. *J. Chem. Phys.* **1985**, *82*, 270. For 6−31G* reference: (e) Ditchfield, R.; Hehre, W. J.; Pople, J. A. Self-Consistent Molecular-Orbital Methods. IX. An Extended Gaussian-Type Basis for Molecular-Orbital Studies of Organic Molecules. *J. Chem. Phys.* **1971**, *54* (2), 724. (f) Hehre, W. J.; Ditchfield, R.; Pople, J. A. Self—Consistent Molecular Orbital Methods. XII. Further Extensions of Gaussian—Type Basis Sets for Use in Molecular Orbital Studies of Organic Molecules. *J. Chem. Phys.* **1972**, *56*, 2257. (g) Clark, T.; Chandrasekhar, J.; Spitznagel, G. W.; Schleyer, P. V. R. Efficient diffuse function-augmented basis sets for anion calculations. III. The 3−21+G basis set for first-row elements, Li−F. *J. Comput. Chem.* **1983**, *4*, 294. For SMD reference: (h) Marenich, A. V.; Cramer, C. J.; Truhlar, D. G. Universal Solvation Model Based on Solute Electron Density and on a Continuum Model ofthe Solvent Defined by the Bulk Dielectric Constant and Atomic Surface Tensions. *J. Phys. Chem. B* **2009**, *113*, 6378. For Gaussian 16 reference: (i) Frisch, M. J.; Trucks, G. W.; Schlegel, H. B.; Scuseria, G. E.; Robb, M. A.; Cheeseman, J. R.; Scalmani, G.; Barone, V.; Petersson, G. A.; Nakatsuji, H.; Li, X.; Caricato, M.; Marenich, A. V.; Bloino, J.; Janesko, B. G.; Gomperts, R.; *Gaussian 16*, Revision C.01; Gaussian Inc., 2016 For def2-TZVP reference: (j) Weigend, F.; Ahlrichs, R. Balanced basis sets of split valence, triple zeta valence and quadruple zeta valence quality for H to Rn: Design and assessment of accuracy. *Phys. Chem. Chem. Phys.* **2005**, *7*, 3297.
(26) Hehre, W. J.; Ditchfield, R.; Pople, J. A. Self−Consistent Molecular Orbital Methods. XII. Further Extensions of Gaussian−Type Basis Sets for Use in Molecular Orbital Studies of Organic Molecules. *J. Chem. Phys.* **1972**, *56*, 2257−2261.
(27) Weigend, F. Accurate Coulomb-fitting basis sets for H to Rn. *Phys. Chem. Chem. Phys.* **2006**, *8*, 1057−1065.
(28) Tresca, B. W.; Brueckner, A. C.; Haley, M. M.; Cheong, P. H.-Y.; Johnson, D. W. Computational and Experimental Evidence of Emergent Equilibrium Isotope Effects in Anion Receptor Complexes. *J. Am. Chem. Soc.* **2017**, *139*, 3962−3965.
(29) Churchill, D. G.; Janak, K. E.; Wittenberg, J. S.; Parkin, G. Normal and Inverse Primary Kinetic Deuterium Isotope Effects for C−H Bond Reductive Elimination and Oxidative Addition Reactions of Molybdenocene and Tungstenocene Complexes: Evidence for Benzene σ-Complex Intermediates. *J. Am. Chem. Soc.* **2003**, *125*, 1403.

https://doi.org/10.1021/acscatal.5c05612
ACS Catal. 2025, 15, 21077−21087